Analysis of Interfacial Cracking in Flip Chip Packages With Viscoplastic Solder Deformation

M. J. Heffes

H. F. Nied
e-mail: hfn2@lehigh.edu

Department of Mechanical Engineering and Mechanics,
Lehigh University,
Bethlehem, PA 18015-3085

This paper examines the modeling of viscoplastic solder behavior in the vicinity of interfacial cracking for flip chip semiconductor packages. Of particular interest is the relationship between viscoplastic deformation in the solder bumps and any possible interface cracking between the epoxy underfill layer and the silicon die. A 3-D finite element code, developed specifically for the study of interfacial fracture problems, was modified to study how viscoplastic solder material properties would affect fracture parameters such as strain energy release rate and phase angle for nearby interfacial cracks. Simplified two-layer periodic symmetry models were developed to investigate these interactions. Comparison of flip chip results using different solder material models showed that viscoplastic models yielded lower stress and fracture parameters than time independent elastic-plastic simulations. It was also found that adding second level attachment greatly increases the magnitude of the solder strain and fracture parameters. As expected, the viscoplastic and temperature dependent elastic-plastic results exhibited greater similarity to each other than results based solely on linear elastic properties. [DOI: 10.1115/1.1649242]

Introduction

Solder joint integrity is recognized as a key issue in the reliability of Flip Chip (FC) and Ball Grid Array (BGA) Integrated Circuit (IC) Packages. In a flip chip package, the silicon die's tiny solder joints are bonded directly to a substrate, which is usually a polymeric composite. In addition, the bond is further reinforced with epoxy underfill that encapsulates the solder joints. This technology is used in applications where high pin count density is needed. The relatively large coefficient of thermal expansion (CTE) mismatch between the die and the substrate can result in high shear and peeling stresses at the corner fillets and edges of the package. Under certain conditions, these stresses are of sufficient magnitude to cause the interfaces to delaminate. A typical failure pattern observed in flip chip packages during thermal cycling, is initial interface delamination, usually between the silicon die and the underfill, followed by fatigue failure of the solder joints. Thus, the two mechanical failure mechanisms that are of primary concern when accessing the reliability of flip chip packages are: 1) interface cracking and 2) failure due to excessive and repeated solder deformation. Clearly, the two failure mechanisms can be interrelated, especially when interface cracking is in close proximity to the solder connections.

Solder joint reliability and the associated modeling techniques for life prediction in flip chip packages have been extensively studied, e.g., [1–10]. The vast majority of this research has focused on solder deformation in uncracked flip chip packages using both 2-D and 3-D finite element models. A smaller subset of the flip chip reliability literature has examined solder joint failure coupled with nearby interfacial cracking [11–14]. The finite element models used in these studies have been essentially two-dimensional, i.e., plane strain. The problem with a plane strain formulation is that all displacements normal to the cross-section of the package are zero. In thermal stress problems, this constraint can cause a large stress component normal to the plane, which in turn may unrealistically affect the conditions for yielding and continued plastic deformation. Unfortunately, a more realistic full 3-D model of the solder structures in the package also requires the introduction of a 3-D interface crack into the solder/crack interaction model. Since most techniques readily available for modeling cracks using the finite element method require a refined and focused mesh at the crack tip, the resulting 3-D fracture model can represent a significant computational challenge. Enriched crack tip element formulations [15–17] offer an alternative approach for modeling interface cracks that do not require any special crack tip meshing. In [18], Ayhan and Nied studied 3-D interaction effects for various types of interface cracks approaching solder connections in a flip chip package. However, in [18], the solder was modeled as a temperature dependent elastic-plastic material, not a viscoplastic material.

In this paper the same 3-D enriched crack tip formulation outlined in [17,18] is utilized, with the addition of localized viscoplastic solder behavior. Since this study is primarily concerned with examining viscoplastic effects, a number of simplifications were made concerning the geometry of the finite element model. For example, Fig. 1 depicts a two-layer slice model used in this study to model the flip chip geometry. In this model, the solder bumps are simply modeled as curved "blocks" and not quasi-spherical or cylindrical structures. In general, solder "bumps" have complex elongated shapes with reentrant corners at their upper and lower attachment points. The precise contact angle for the joint depends on solder surface tension, surface wetting, and any additional deformation that may occur during cool-down following solder reflow. Detailed localized stresses depend critically on the stress concentrations at these points. However, average stresses through the center plane of the solder bump are not affected by these geometric details. "Extruding" a planar model in the out-of-plane direction (as depicted in Fig. 1) greatly simplifies creation of the two-layer slice model, with both the back and front planes of this model representing planes of periodic symmetry. For example, the back plane in Fig. 1 passes through the center plane of the solder bumps, while the front surface of the model is located on a symmetry plane passing though the underfill material separating two rows of solder bumps. In the 3-D model depicted in Fig. 1, nodes located on the front surface of the model are constrained to have the same out-of-plane (z) displacement. Thus, unlike plane strain models, thermal expansion is permitted in the out-of-plane direction. It has been shown that such models are very effective for simulating 3-D stress states in the central region of various semiconductor packages, e.g., [18–20].

Viscoplastic models have been successfully used to provide es-

Contributed by the Electronic and Photonic Packaging Division for publication in the JOURNAL OF ELECTRONIC PACKAGING. Manuscript received March 2003; final revision, November 2003. Associate Editor: Z. Suo.

 Copyright © 2004 by ASME

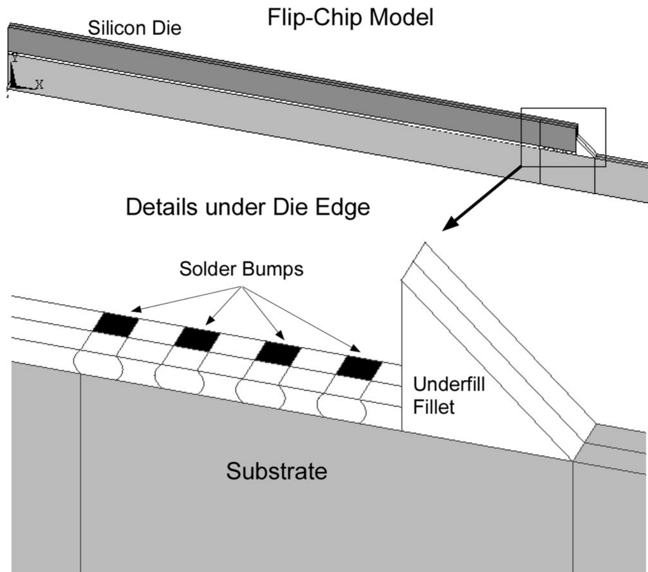

Fig. 1 Schematic diagram of two layer flip chip model

timates of solder bump fatigue life based on empirical relationships that utilize accumulated creep strains or inelastic strain energy density per load cycle [19–24]. In addition, fatigue life estimates for cracks growing on interfaces can be calculated using empirical relationships based on crack growth rates as a function of cyclic changes in the strain energy release rate (ΔG), for given ratios of mode II to mode I stress intensity factors. For example, Snodgrass et al., [25], provide relevant crack growth data for polymer/silica interfaces subjected to various environmental conditions. Comparison of life estimates based on these different failure mechanisms, i.e., solder fatigue and interfacial crack growth, provides a powerful methodology for predicting package reliability. However, this approach relies heavily on accurate numerical simulation of viscoplastic deformation in solder, as well as simultaneous calculation of interface fracture parameters, i.e., strain energy release rate and stress intensity factors.

Interfacial Crack FEM Using Enriched Elements

In this study, enriched crack tip elements are used to accurately compute stress intensity factors along a 3-D crack front. The enriched finite element formulation for interface crack problems is an extension of concepts introduced by Benzley [26] for conventional isotropic fracture problems. Application of the enrichment technique to interfacial fracture problems is relatively straightforward for two-dimensional problems once the asymptotic crack tip displacement and strain fields have been derived. For example, enriched crack tip elements have been formulated for interface cracks between dissimilar isotropic [15] and orthotropic [16] media. The enriched crack tip elements contain the closed-form asymptotic solutions for displacements and strains in addition to the usual polynomial interpolation functions. Following this approach, the stress intensity factors are additional degrees of freedom computed directly in the same manner as the nodal displacements. One advantage of this approach is that there is no need for a special crack tip mesh, e.g., refined "tunnel" mesh or relocation of nodes to obtain singular stresses. As long as the enriched elements are properly integrated and transition elements are used to maintain displacement compatibility, automatically generated, unrefined meshes are adequate for highly accurate results.

In [27,28] these concepts were extended to 3-D crack problems. The expressions for the displacement field for enriched 3-D elements are given by [27]

$$u(\xi,\eta,\rho)=\sum_{j=1}^{r} N_j(\xi,\eta,\rho)u_j+Z_0(\xi,\eta,\rho)\{K_I(\Gamma)F_1(\xi,\eta,\rho)+K_{II}(\Gamma)G_1(\xi,\eta,\rho)+K_{III}(\Gamma)H_1(\xi,\eta,\rho)\} \quad (1)$$

$$v(\xi,\eta,\rho)=\sum_{j=1}^{r} N_j(\xi,\eta,\rho)v_j+Z_0(\xi,\eta,\rho)\{K_I(\Gamma)F_2(\xi,\eta,\rho)+K_{II}(\Gamma)G_2(\xi,\eta,\rho)+K_{III}(\Gamma)H_2(\xi,\eta,\rho)\} \quad (2)$$

$$w(\xi,\eta,\rho)=\sum_{j=1}^{r} N_j(\xi,\eta,\rho)w_j+Z_0(\xi,\eta,\rho)\{K_I(\Gamma)F_3(\xi,\eta,\rho)+K_{II}(\Gamma)G_3(\xi,\eta,\rho)+K_{III}(\Gamma)H_3(\xi,\eta,\rho)\}. \quad (3)$$

In Eqs. (1)–(3), u_j, v_j and w_j represent the r unknown nodal displacements and $N_j(\xi,\eta,\rho)$ are the conventional element shape functions in terms of the element's local coordinates (ξ,η,ρ). $K_I(\Gamma),K_{II}(\Gamma),K_{III}(\Gamma)$ represent the mode I, II, and III, stress intensity factors varying along the crack front defined by the interpolation functions $N_i(\Gamma)$. For a 20-noded hexahedron, with three crack tip nodes, the stress intensity factors are interpolated using the quadratic polynomial shape function associated with the displacements at these same nodes. In the enriched crack tip element Z_0 is identically equal to 1. However, in elements adjacent to the crack tip elements, Z_0 plays the role of a "zeroing function," providing inter-element compatibility between the crack tip elements and the regular elements that surround the enriched elements [27]. In a typical transition element, $Z_0=1$ at all points where the transition element is in contact with a crack tip element, and is zero along sides, edges and points coincident with regular isoparametric elements.

The functions F_i, G_i, and H_i, contain the asymptotic terms, that when multiplied by the constant K_I,K_{II},K_{III}, form the asymptotic crack tip displacements. For example, these terms are given in [15] for an interface crack between two isotropic materials. It is well known that the singular, elastic stress field near the tip of an interface crack is different than a crack in a homogeneous material, exhibiting an oscillatory behavior close to the crack tip. The singular stress field for an interface crack is given by

$$\sigma_{ij}=\frac{1}{\sqrt{2\pi r}}\{\mathrm{Re}[Kr^{i\varepsilon}]\tilde{\sigma}^{I}_{ij}(\theta,\varepsilon)+\mathrm{Im}[Kr^{i\varepsilon}]\tilde{\sigma}^{II}_{ij}(\theta,\varepsilon)+K_{III}\tilde{\sigma}^{III}_{ij}(\theta)\} \quad (4)$$

where $i=\sqrt{-1}$ and r, θ define polar coordinates in a local coordinate system perpendicular to the crack front. In Eq. (4) the complex stress intensity factor K is defined as K_I+iK_{II} and $\tilde{\sigma}_{ij}$'s are the angular stress variation terms for different modes of loading. The complex power in Eq. (4) depends on the properties of the constituent interface materials, through the oscillatory index ε, given by

$$\varepsilon=\frac{1}{2\pi}\ln\left[\frac{1-\beta}{1+\beta}\right]. \quad (5)$$

In Eq. (5) β is the second Dundurs' parameter. Dundurs' parameters, used to characterize bimaterial problems, are defined by

$$\alpha=\frac{\mu_1(\kappa_2+1)-\mu_2(\kappa_1+1)}{\mu_2(\kappa_1+1)+\mu_1(\kappa_2+1)}, \quad \beta=\frac{\mu_1(\kappa_2-1)-\mu_2(\kappa_1-1)}{\mu_2(\kappa_1+1)+\mu_1(\kappa_2+1)} \quad (6)$$

with μ the shear modulus and $\kappa=3-4\nu$ (ν is Poisson's ratio). The subscripts for μ, κ, and ν in (6) identify the different materials on either side of the interface. In [28] example 3-D interface fracture results are presented for interface cracks between silicon and epoxy using the enriched finite element procedure described above.

Table 1 Flip chip elastic material properties

	Elastic Modulus (MPa)		CTE× 10^6 /°C		Poisson's Ratio
	@25°C	@150° C	@25° C	@150 °C	
Silicon	131,000	131,000	2.8	2.8	0.28
Substrate	17,700	14,900	15	15	0.39
Underfill	4,800	2,200	24	49	0.33
Solder	29,600	10,290	23.3	23.3	0.35
Underfill solder mix	11,000	4,200	28	49	0.33

For the silicon/epoxy materials used in this study (see Table 1), Dundurs' parameters are given by $\alpha=0.9270$, $\beta=0.2333$ and the oscillatory index $\varepsilon=-0.0756$.

Viscoplastic Model

A variety of viscoplastic constitutive models have been developed to simulate creep deformation behavior in solder. Since electronic packages are subjected to thermal cycling conditions that often result in relatively short stress relaxation times, viscoplastic models that include transient (primary creep) behavior are generally preferred over simple steady state creep models. For example, assuming a von Mises yield criterion, Lau [29], provides curve fits to solder data, obtained from extensive testing on a number of different solder alloys, using the following viscoplastic (time dependent plasticity) relationship for the uniaxial equivalent creep strain rate $d\varepsilon_c/dt$

$$\frac{d\varepsilon_c}{dt}=\frac{d\varepsilon_s}{dt}(1+C_5C_6\exp(-C_5\bar{\varepsilon}_{VP})), \tag{7}$$

where $d\varepsilon_s/dt$ represents the uniaxial equivalent steady state creep strain rate given by,

$$\frac{d\varepsilon_s}{dt}=C_1[\sinh(C_2\sigma)]^{C_3}\exp(-C_4/T). \tag{8}$$

In Eqs. (7) and (8), $\bar{\varepsilon}_{VP}$ is the effective transient viscoplastic creep strain, σ the effective stress, and T the absolute temperature in degrees Kelvin. The six constants in Eqs. (7) and (8) are reproduced from [29] in Table 2. In this study, the finite element implementation of the viscoplastic model implied by Eqs. (7) and (8), closely follows the procedure outlined in [30]. The total strain is assumed to be the sum of the elastic, thermal and viscoplastic creep strains, i.e.,

$$\varepsilon_T=\varepsilon_e+\varepsilon_{Th}+\varepsilon_c \tag{9}$$

The finite element solution for the nonlinear system of equations is essentially the same approach developed for incremental plasticity, where implicit time integration is used and at each time increment, load equilibrium is reestablished through successive iterations. Specific details related to the finite element formulation used in this study are given in [30,31].

Table 2 Solder viscoplastic constants [29]

	Units	Sn60Pb40	62Sn36Pb2Ag
C1	1/sec	1.61E+05	8.03E+04
C2	1/psi	4.62E−04	4.62E−04
C2	1/MPa	0.067007	0.067007
C3		3.3	3.3
C4	Deg K	8112	8112
C5		698	263
C6		0.015	0.023

Flip Chip Model

A flip chip model with interfacial cracks will be used to demonstrate computation of time dependent stress intensity factors, coupled with the solder creep behavior. For simplicity, the model used in this study is a periodic symmetry model consisting of two layers, one of which contains solder bumps and underfill, while the other layer contains only underfill between the silicon and substrate layers (see Figs. 1 and 2). Table 3 gives the dimension of the geometric features in this model. The two-layer slice model was created by extruding a 2-D mesh out of the plane, as shown in Fig. 2. The volume of the solder was estimated based on the average volume through the solder bump cross-section assuming a cylindrical shape. This solder volume was then preserved in the extruded model. The back plane of this model represents a symmetry plane that passes through the center of the solder bump structures, while the front plane represents a symmetry plane equidistant between rows of solder bumps. In the two-layer model, all of the out-of-plane displacements u_z on the front plane in Fig. 2 are constrained to be equal. Two types of cracks (Fig. 3) were investigated in this study: a) A vertical fillet crack located on the vertical interface between the silicon die and the underfill fillet

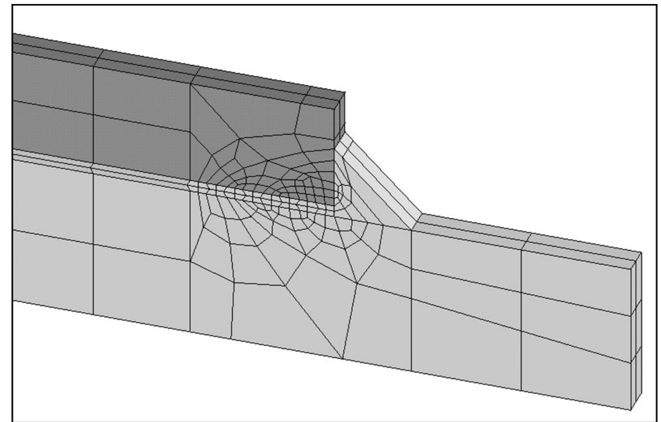

Fig. 2 Finite element mesh for two layer flip chip model

Table 3 Flip chip model dimensions

Feature	Length in mm	Feature	Length in mm
Die Half-Length	14.400	Underfill Layer Thickness	0.100
Substrate Half-Length	16.270	Solder Layer Thickness	0.100
Fillet Side Lengths	0.381	Solder Bump Pitch	0.325
Die Height	0.686	Solder Bump Minimum Width	.100
Substrate Height	1.000	Solder Bump Maximum Width	.140
Underfill/Solder Height	0.076	Fillet Crack Length	0.165

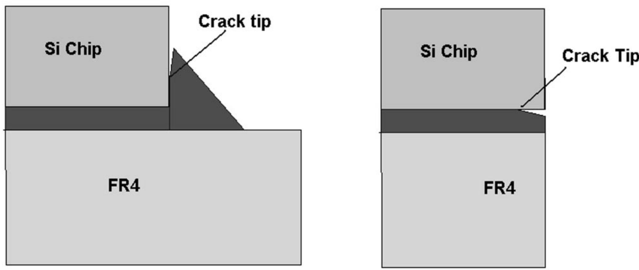

Fig. 3 Schematic showing location of: (*a*) vertical fillet edge crack and (*b*) horizontal crack underneath chip.

(crack length $a=0.165$ mm), and b) A horizontal crack on the horizontal surface between the silicon die and the underfill/solder layer ($a=0.07$ mm). In the later case, the fillet was omitted from the model, since the horizontal edge crack in reality will take the form of an "L" shaped crack, if it is a continuation of the vertical fillet crack propagating around the edge of the die. Such cracks were investigated in [18] and were found to be quite similar to horizontal edge cracks, but the "L" shaped crack introduces a more complex behavior associated with crack surface contact that is not examined in this study.

Comparison of Viscoplastic, Elastic-Plastic, and Linear Elastic Results

The model described in the previous section was used to compute stress intensity factors for cracked packages subjected to uniform temperature changes. In these calculations, 150°C was specified as the stress free reference temperature. This represents the temperature at which solder reflow and underfill cure are completed during manufacturing. Subjecting the package to a uniform $\Delta T=-125$°C brings the package down to a final temperature of 25°C. In the elastic-plastic and viscoplastic models, the mechanical behavior of the solder is strongly temperature dependent. In addition, the uniaxial yield stress depends on strain rate. Thus, for comparison purposes, in the elastic-plastic calculations, the yield stress was specified as the stress level that would cause a strain of 0.005, 5 minutes after sudden application of a step load. The magnitude of this uniaxial yield stress was determined using the viscoplastic model defined by Eqs. (7) and (8) and the data given in Table 2. For example, Table 4 lists the yield stress values that were obtained in this manner for the 62Sn36Pb2Ag solder data listed in Table 2.

For the flip-chip model shown in Fig. 2, the mechanical response during uniform cooling, was first simulated for an unconstrained package, cooled from 150°C to 25°C in a 300 second time period ($\Delta T=0.4167$°C/s). Figure 4 shows the results from such a calculation with the temperature profile, demonstrating the difference between the time independent elastic-plastic model and the viscoplastic thermomechanical simulation. In Fig. 4 the Von Mises stresses in the center of the outer-most solder bump are plotted as a function of time using both constitutive models. Not surprisingly, the viscoplastic model exhibits somewhat lower stresses throughout the simulation. In addition, upon reaching 25°C, the viscoplastic model exhibits significant stress relaxation in contrast to the elastic-plastic model.

Table 4 Solder yield strengths used for time independent plastic analysis (62Sn36Pb2Ag)

Temp (°K)	Yield Strength (MPa)
298	26.67
350	11.53
423	4.00

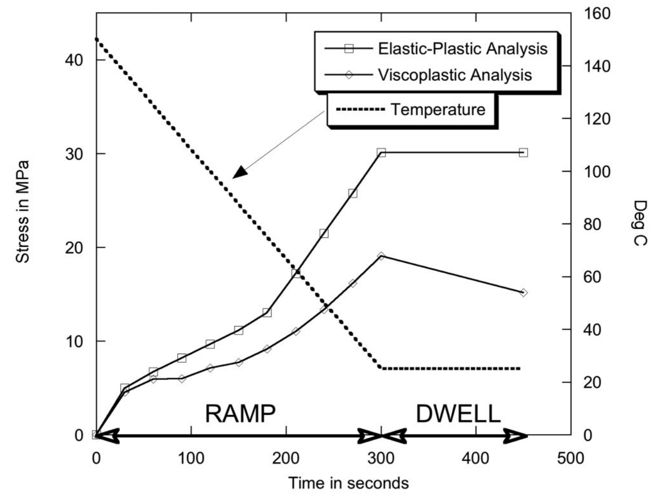

Fig. 4 Comparison of Von Mises stresses for elastic-plastic and viscoplastic models in the center of the outer-most solder bump

Figure 5 shows the associated viscoplastic and plastic effective strains at the same location. The deformation behavior is very similar in these two cases, i.e., the solder deformation is primarily controlled by the mechanical constraints of the surrounding elastic material. One difference between the two models can be seen in the continued creep deformation of the viscoplastic material during the dwell time. Even though the solder exhibits both creep and stress relaxation behavior during the dwell time, the creep behavior at the final temperature is relatively small. In the elastic-plastic case, the magnitude of the effective stress is equal to the uniaxial yield stress at every point on the curve during cooling and primarily reflects the interpolated temperature dependent yield stress behavior provided by Table 4.

Figure 6 depicts the strain energy release rate for a vertical fillet crack (Fig. 3a), of length $a=0.165$ mm, at a point on the crack front lying in the plane of symmetry of the solder bumps, i.e., the back plane of Figs. 1 and 2. The magnitude of the strain energy release rate for the linear elastic case (dashed line) is $G=0.270$ J/m^2 after cool down. In comparison to the linear elastic

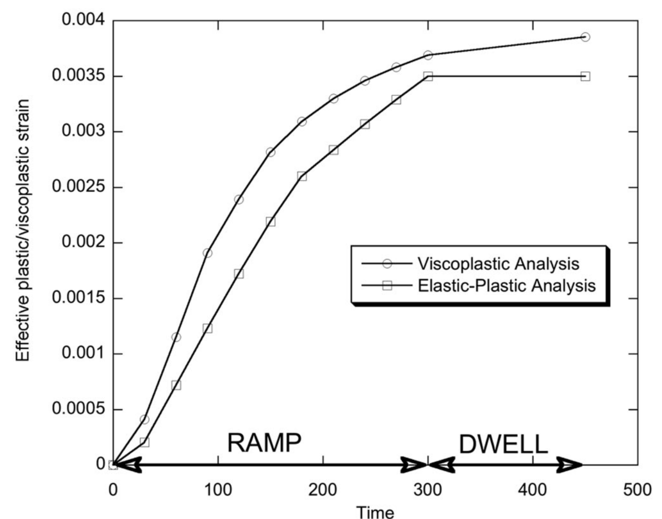

Fig. 5 Comparision of effective plastic strain for the elastic-plastic and viscoplastic models in the center of outer-most solder bump

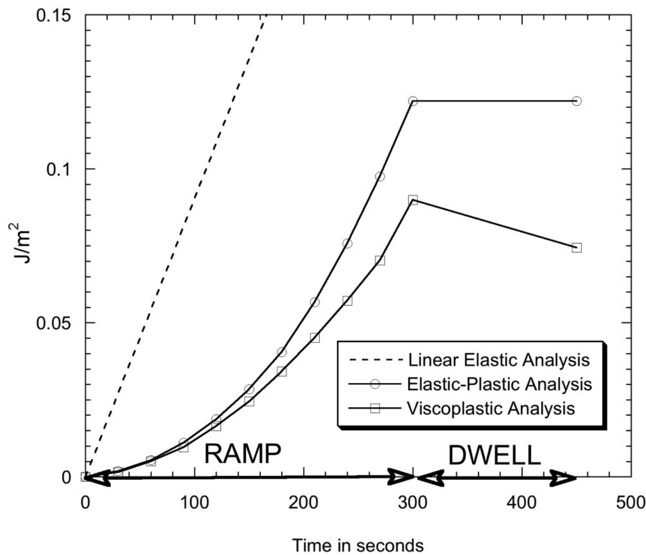

Fig. 6 Comparison of strain energy release rate for vertical fillet crack. Linear elastic, elastic-plastic and viscoplastic cases.

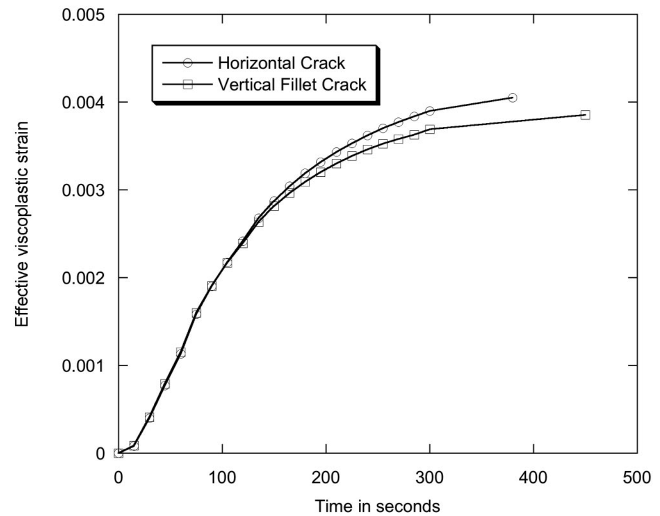

Fig. 8 Viscoplastic strain in the solder. Comparison between vertical fillet and horzontal crack cases.

fracture model, the strain energy release rate for the elastic-plastic and viscoplastic models is a nonlinear function of temperature that decreases with increasing stress relaxation in the solder. This can be clearly seen during the dwell period, as the energy release rate decreases for the viscoplastic model, but remains constant for the elastic-plastic model. Figure 7 shows the phase angle Ψ at the same point on the crack front. For an interface crack, Ψ is defined in terms of the mode II and mode I stress intensity factors as

$$\psi = \tan^{-1}\frac{K_{II}}{K_I}, \tag{10}$$

where K_I and K_{II} are the real and imaginary parts or the complex stress intensity factor defined in Eq. (4). For example, the stresses directly ahead of the crack tip, expressed in terms of complex K are given by

$$\sigma_{22} + i\sigma_{12} = \frac{1}{\sqrt{2\pi r}} K r^{i\varepsilon}. \tag{11}$$

It can be seen from Fig. 7 that this phase angle or mode mixity is not significantly affected by the differences between the plastic and viscoplastic material models. It should also be noted that a portion of the variation in Ψ and G is attributed to the temperature dependence of the underfill properties.

A second, horizontal crack, model was created to simulate a crack that has propagated past the fillet to a point underneath the Si chip (Fig. 3(b)) 0.07 mm from the bottom corner of the die. Thus, the crack tip is much closer to the outer-most solder bump. In this case, one would expect that the interaction effects between the solder bump and the crack would be more pronounced. It is interesting to note that the closer proximity of the crack tip has very little effect on the creep behavior of the outer-most solder bump (Fig. 8). Figure 8 shows that the creep behavior in the solder differs only slightly for the two different crack geometries shown in Fig. 3. The effect on the crack tip fracture parameters is more pronounced. Figure 9 compares the strain energy release rates between the vertical fillet crack and the horizontal sub-die

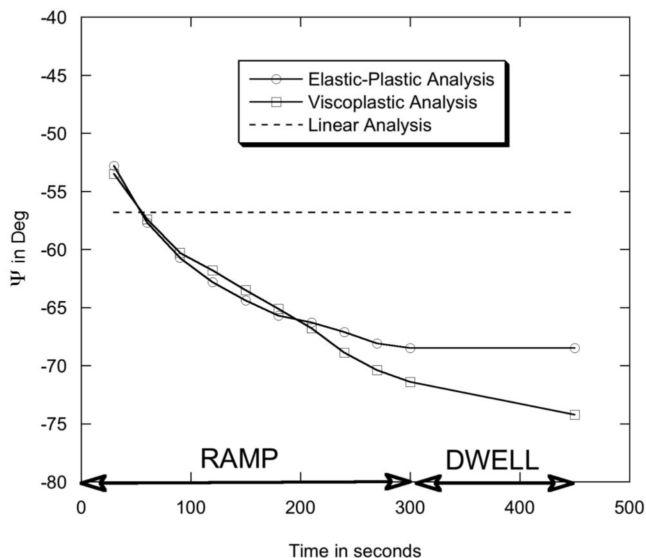

Fig. 7 Comparison of phase angle for vertical fillet crack. Linear elastic, elastic-plastic and viscoplastic cases.

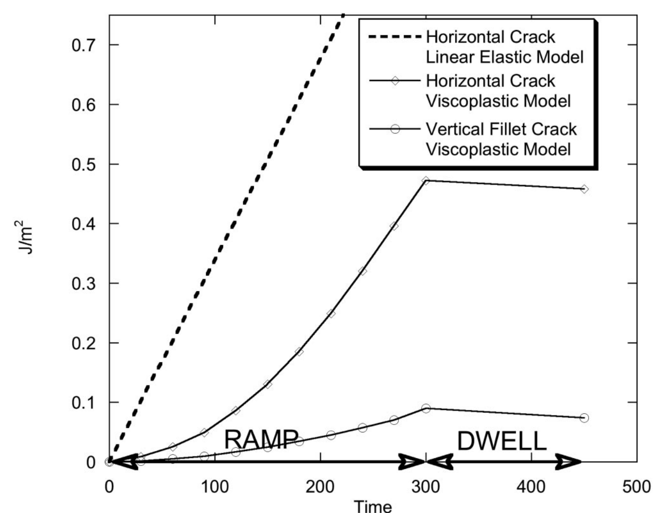

Fig. 9 Strain energy release rate comparisons. Vertical fillet crack and horizontal crack.

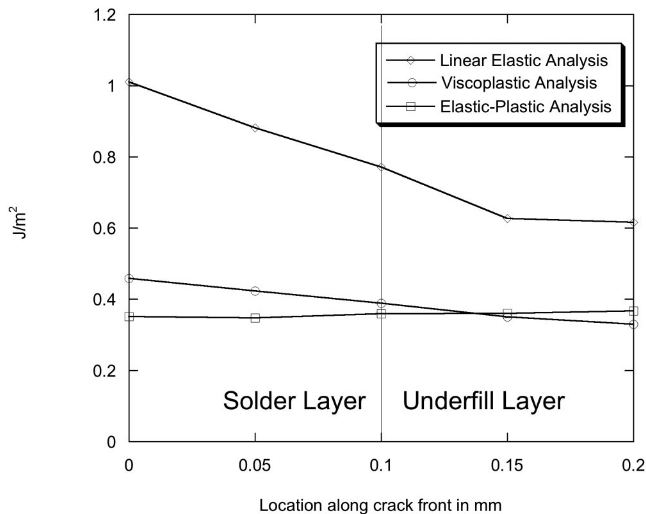

Fig. 10 Variation in strain energy release rate along the crack front in severe crack model

crack. The magnitude of the strain energy release rate for the crack underneath the Si die in the linear elastic case (dashed line) is $G = 1.0\ \mathrm{J/m^2}$. Thus, the horizontal crack should be considered more severe than the previous model with a vertical crack. This behavior is also seen in the viscoplastic results, where the horizontal crack's energy release rate is about five times greater than the vertical fillet crack's energy release rate after cool down. Figure 10 depicts the 3-D nature of the strain energy release rate along the crack front for the horizontal crack case. In the linear elastic calculation, the strain energy release rate decreases from a maximum of $\sim 1.0\ \mathrm{J/m^2}$ at the point on the crack front closest to the solder bump, to $\sim 0.6\ \mathrm{J/m^2}$ in where the crack front is located in the center of the underfill only region. In the viscoplastic case, the energy release rate is only slightly higher at the point where the crack front is closest to the solder bump and in the elastic-plastic case the energy release rate is essentially constant along the crack front. Calculations performed in [18] using the elastic-plastic model, showed that the nature of the strain energy release rate variation along the crack front depends very strongly on how close the crack front is to the solder bump, i.e., the closer the crack is to solder bump, the greater the magnitude of the strain energy release rate at that point on the crack front. In the example depicted in Fig. 10, the crack is not close enough to the solder bump to see a strong variation in the nonlinear models. One would expect more significant 3-D effects if the crack tip were moved closer to the outer-most solder bump.

Flip Chip With Second Level Attach

The previous results were obtained without any external constraints on the flip chip package during cooling. However, it is generally believed that the mechanical constraints imposed by second level attachment (BGA solder balls and a circuit board) can have a major impact on first level reliability. In an effort to examine the nature of the constraints imposed by second level attachment, a simple model was constructed with two extra layers below the substrate in the original model (Fig. 11). The layer directly below the substrate represents an array of BGA solder balls and the bottom-most layer a PCB. The BGA solder layer was modeled as a "smeared" viscoplastic material with a composition made up of approximately 40% solder and 60% air. Table 5 contains the dimensions and material properties that were used to simulate the effects of second level attachment.

Figures 12 and 13 show the increased viscoplastic strain experienced by the solder bumps under the flip chip as well as the strain energy release rate for the vertical fillet crack, in a package

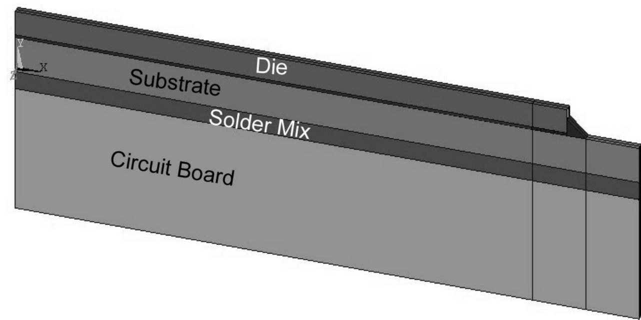

Fig. 11 Schematic of flip chip cross-section with second level attachment. Vertical fillet crack located in upper right corner.

subjected to second level attachment constraints. Figure 12 also shows the magnitude of the effective viscoplastic strain on the outermost edge of the solder mix layer that represents the BGA attachment. The results indicate that the magnitude of the effective viscoplastic strain in the flip chip solder bump, under the die edge, is 47% greater under these conditions. Similarly, the strain energy release rate for the small vertical fillet crack is an order of magnitude greater than the results obtained from the unconstrained (unattached) model. This simple example clearly demonstrates that the additional mechanical constraints associated with second level attachment can have a significant effect on both the viscoplastic and interface fracture behavior.

Conclusions

A viscoplastic capability, implemented in a specialized 3-D finite element program for fracture mechanics applications, was used to examine certain time dependent interaction effects between solder structures and interfacial cracking. Example flip chip

Table 5 Second level attachment dimensions and properties

	Young's Modulus (MPa)	CTE ($10^{-6}/°C$)	Poisson's Ratio	Layer Thickness (mm)
Solder Mix	11,000	23.3	.33	0.5
PCB	28,300	15	.39	4

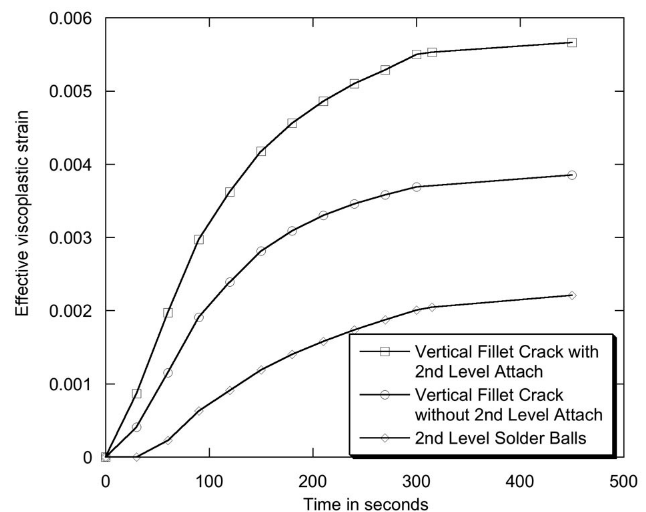

Fig. 12 Effective strains in outermost solder structures showing the effect of second level attachment. Vertical fillet crack case.

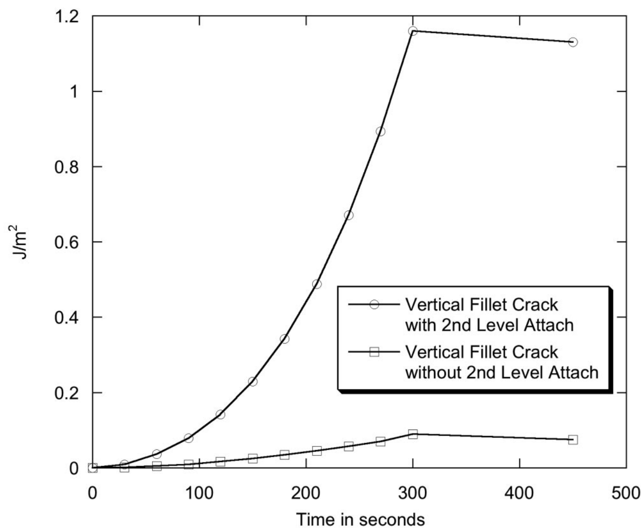

Fig. 13 Strain energy release rate for vertical fillet crack showing the effect of second level attachment

models were used to demonstrate the differences between processing simulations using different nonlinear material models for the solder structures, e.g., elastic-plastic vs. viscoplastic. The results indicate that even though the viscoplastic models may provide a more accurate description of the material behavior, the results are very similar to those obtained from the temperature dependent elastic-plastic models for the simple cool-down thermal loading examined in this study. One would expect more significant differences for simulations with dwell times at elevated temperatures. The dwell period at 25°C did not have a significant effect on the strain levels or fracture parameters. Time dependent interaction effects between interfacial cracks and the solder bumps are also very slight, unless the crack tip is in very close proximity to the solder bump. This is similar to results obtained in [18] using elastic-plastic models.

Finally, addition of second level attachment has a fairly significant impact on the viscoplastic behavior of the solder bumps in the flip chip and any potential cracking behavior on the interface between the silicon die and the underfill fillet. This suggests that analysis of flip chip attachment to the board is an important consideration when trying to estimate the reliability of flip chip packages.

Acknowledgment

The support of the Semiconductor Research Corporation (SRC) under grant SRC 826.002 is gratefully acknowledged.

References

[1] Schubert, A., Dudek, R., Auersperg, J., Vogel, D., Michel, B., and Reichl, H., 1997, "Thermo-Mechanical Reliability Analysis of Flip Chip Assemblies by Combined Microdac and the Finite Element Method," *ASME EEP-Vol. 12-2, Advances in Electronic Packaging*, Vol. 2, pp. 1647–1654.
[2] Wang, J., Qian, Z., and Liu, S., 1998, "Process Induced Stresses of a Flip-Chip Packaging by Sequential Processing Modeling Technique," ASME J. Electron. Packag., **120**, pp. 309–313.
[3] Darbha, K., Okura, J. H., Shetty, S., Dasgupta, A., Reinikainen, T., Zhu, J., and Caers, J. F. J. M., 1999, "Thermomechanical Durability Analysis of Flip Chip Solder Interconnects: Part 2-With Underfill," ASME J. Electron. Packag., **121**, pp. 237–241.
[4] Zhu, J., 1999, "Three-Dimensional Effects of Solder Joints in Mircro-Scale BGA Assembly," ASME J. Electron. Packag., **121**, pp. 297–302.
[5] Yao, Q., and Qu, J., 1999, "Three-Dimensional Versus Two-Dimensional Finite Element Modeling of Flip-Chip Packages," ASME J. Electron. Packag., **121**, pp. 197–201.
[6] Yao, Q., Qu, J., and Wu, S. X., 1999, "Thermomechanical Fatigue Life of Chip Scale Packages," *ASME EEP-Vol. 26-2, Advances in Electronic Packaging*, Vol. 2, pp. 1533–1538.
[7] Lau, J. H., 1999, "Three Dimensional Elastoplastic and Creep Analysis of a Low Cost Solder-Bumped Flip-Chip Chip Scale Package (CSP) Assembly," *ASME EEP-Vol. 26-2, Advances in Electronic Packaging*, Vol. 2, pp. 1093–1098.
[8] Tsukada, Y., Nishimura, H., Sakane, M., and Ohnami, M., 2000, "Fatigue Life Analysis of Solder Joints in Flip Chip Bonding," ASME J. Electron. Packag., **122**, pp. 207–213.
[9] Lu, H., Bailey, C., and Cross, M., 2000, "Reliability Analysis of Flip Chip Designs Via Computer Simulation," ASME J. Electron. Packag., **122**, pp. 214–219.
[10] Darbha, K., and Dasgupta, A., 2001, "A Nested Finite Element Methodology (NFEM) for Stress Analysis of Electronic Products-Part II: Durability Analysis of Flip Chip and Chip Scale Interconnects," ASME J. Electron. Packag., **123**, pp. 147–155.
[11] Rzepka, S., Korhonen, M. A., Meusel, E., and Li, C.-Y., 1998, "The Effect of Underfill and Underfill Delamination on the Thermal Stress in Flip-Chip Solder Joints," ASME J. Electron. Packag., **120**, pp. 342–348.
[12] Lau, J. H., and Ricky Lee, S.-W., 2000, "Fracture Mechanics Analysis of Low Cost Solder Bumped Flip Chip Assemblies with Imperfect Underfills," ASME J. Electron. Packag., **122**, pp. 306–310.
[13] Lau, J. H., 2000, *Low Cost Flip Chip Technologies*, McGraw-Hill.
[14] Gu, Y., Nakamura, T., Chen, W., and Cotterell, B., 2001, "Interfacial Delamination Near Solder Bumps and UBM in Flip-Chip Packages," ASME J. Electron. Packag., **123**, pp. 295–301.
[15] Chen, E. P., 1985, "Finite Element Analysis Of A Bimaterial Interface Crack," *Theoretical and Applied Fracture Mechanics*, Vol. 3, pp. 257–262.
[16] Kaya, A. C., and Nied, H. F., 1993, "Interface Fracture Analysis Of Bonded Ceramic Layers Using Enriched Finite Elements," *Ceramic Coatings*, K. Kokini, ed., *ASME MD-Vol. 44*, pp. 47–71.
[17] Ayhan, A. O., and Nied, H. F., 1999, "Finite Element Analysis of Interface Cracking in Semiconductor Packages," IEEE Transactions on Components and Packaging Technology, **22**, pp. 503–511.
[18] Ayhan, A. O., and Nied, H. F., 2000, "Finite Element Modeling of Crack Interactions with Solder Balls," *Proceedings of SEM IX International Congress on Experimental Mechanics*, pp. 889–894, Orlando, FL.
[19] Darveaux, R., 2000, "Effect of Simulation Methodology on Solder Joint Crack Growth Correlation," *50th Electronic Components and Technology Conference 2000*, pp. 1048–1058, Las Vegas, NV.
[20] Nagaraj, B., 1999, "OMPAC Package C5 Reliability-Parametric Study," ASME J. Electron. Packag., **121**, pp. 18–22.
[21] Anderson, T., Guven, I., Madenci, E., and Gustasson, G., 1999, "The Necessity of Reexamining Previous Life Prediction Analyses of Solder Joints in Electronic Packages," *49th Electronic Components and Technology Conference*, pp. 1010–1014.
[22] Anderson, T., Barut, A., Guven, I., and Madenci, E., 2000, "Revisit of Life-Prediction Model for Solder Joints," *50th Electronic and Components and Technology Conference*, pp. 1064–1069.
[23] Pang, J. H. L., Tan, T-I, and Sitaraman, S. K., 1998, "Thermo-Mechanical Analysis of Solder Joint Fatigue and Creep in a Flip Chip On Board Package Subjected to Temperature Cycling Loading," *1998 Electronic Components and Technology Conference*, IEEE, pp. 878–883.
[24] Clech, J-P, 1998, "Flip Chip/CSP Assembly Reliability and Solder Volume Effects," *Proc. 1998 Surface Mount International Conference*, San Jose, CA.
[25] Snodgrass, J. M., Pantelidis, D., Jenkins, M. L., Bravman, J. C., and Dauskardt, R. H., 2002, "Subcritical Debonding of Polymer/Silica Interfaces under Monotonic and Cyclic Loading," Acta Mater., **50**(9), 2395–2411.
[26] Benzley, S. E., 1974, "Representation of Singularities with Isoparametric Finite Elements," Int. J. Numer. Methods Eng., **8**, pp. 537–545.
[27] Ayhan, A. O., and Nied, H. F., 2002, "Stress Intensity Factors for Three-Dimensional Surface Cracks using Enriched Finite Elements," Int. J. Numer. Methods Eng., **54**(6), pp. 899–921.
[28] Ayhan, A. O., and Nied, H. F., 2001, "Analysis of Three-Dimensional Interface Cracking in Electronic Packages," *Advances in Fracture Research, Proceedings of ICF10*, K. Ravi-Chandar, B. L. Karihaloo, T. Kishi, R. O. Ritchie, A. T. Yokobori Jr., T. Yokobori, eds., ICF100832OR, Elsevier Science CD-ROM, ISBN 0080440428, December.
[29] Lau, John H., 1995, *Ball Grid Array Technology*, McGraw Hill.
[30] Owen, D. R. J., and Hinton, E., 1980, *Finite Elements in Plasticity*, Pineridge Press.
[31] Heffes, Marc, 2001, "Interfacial Cracking in Flip Chip Packages with Viscoplastic Solder Deformation" M. S. Thesis, Lehigh University, Bethlehem, PA.

View publication stats